(Received 20 February 2025, Accepted 8 April 2025, Scheduled 12 April 2025)

Towards Biosensing and Bioimaging Applications of Gradient Surface Electromagnetic Waves

Igor I. Smolyaninov* and Quirino Balzano

Saltenna LLC, 1751 Pinnacle Dr. Ste. 600, McLean, VA 22102-4007, USA

ABSTRACT: Recently, it was demonstrated that a new type of radio frequency surface electromagnetic wave appears on the surface of a lossy conductive medium in the presence of dielectric permittivity gradients. We present theoretical and experimental study of gradient surface electromagnetic wave (GSEW) excitation and propagation on such conductive surfaces as various metals, water, and human skin. The geometry of our experiments is designed to emulate various potential biosensing and bioimaging applications of GSEW. We demonstrate the capability of GSEW-based techniques to detect the presence of metallic and dielectric objects underwater in close proximity to the water surface. Since the dielectric properties of the human body are similar to those of water, we anticipate that the developed GSEW technique may supplement X-ray and ultrasound-based biosensing and bioimaging.

1. INTRODUCTION

Based on recent theoretical simulations [1], human tissue boundaries and interfaces may support a new type of surface electromagnetic waves that exist in the presence of dielectric permittivity gradients across an interface. The deep subwavelength character of these novel gradient surface electromagnetic waves (GSEWs) appears very beneficial for high resolution biosensing and bioimaging applications. Compared to the existing alternatives, such as X-ray and ultrasound-based sensing and medical imaging techniques, radio frequency GSEWs are supposed to be less harmful to biological tissues, while providing comparable or better spatial imaging resolution — see the detailed data on dielectric properties of human tissues and the detailed numerical simulations reported in [1]. In addition, the contrast mechanism of GSEW techniques (which are mostly sensitive to the dielectric properties of tissues) is manifestly different, which promises added benefits in medical diagnostics. Extreme sensitivity to near surface tumors may be expected due to the well-known extreme sensitivity of surface wave-based techniques in chemical and biological sensing applications [2].

In this paper, we present the theoretical and experimental study of GSEW excitation and propagation on such conductive surfaces as various metals, water, and human skin. We demonstrate that similar types of surface wave antennas may be used for efficient GSEW excitation in all these cases, which makes experimental studies of fundamental GSEW properties in simple model geometries very useful in the context of future biosensing and bioimaging applications. GSEW propagation and scattering in these basic model geometries must be well understood before much more complicated biological systems may be considered.

* Corresponding author: Igor I. Smolyaninov (igor.smolyaninov@saltenna.com).

In particular, we demonstrated the capability of GSEW-based techniques to detect the presence of metallic and dielectric objects underwater in close proximity to the water surface. Since biological tissues are mostly made of water, the geometry of our experiments well represents various simple biosensing and bioimaging situations. We anticipate that in the near future the developed GSEW technique may supplement X-ray and ultrasound-based biosensing and bioimaging.

2. THEORETICAL CONSIDERATIONS

Detailed theoretical derivations of the basic properties of GSEW may be found in the recent reports [1, 3] and an extended tutorial article [4]. In particular, it was demonstrated that the wave equation which describes TM-polarized GSEW propagation along an arbitrary non-magnetic ($\mu = 1$) interface may be reduced to a one-dimensional Schrodinger equation

$$-\frac{\partial^2\psi}{\partial z^2} + \left(-\frac{\varepsilon(z)\omega^2}{c^2} - \frac{1}{2}\frac{\partial^2\varepsilon}{\varepsilon\partial z^2} + \frac{3}{4}\frac{\left(\partial\varepsilon/\partial z\right)^2}{\varepsilon^2}\right)\psi$$

$$= -\frac{\partial^2\psi}{\partial z^2} + V\psi = -k^2\psi \quad (1)$$

where an effective wave function ψ is introduced as $E_z = \psi/\varepsilon^{1/2}$, and the roles of effective potential and total energy are played by the V and $-k^2$ terms, respectively. On the other hand, in the case of TE polarization the wave equation does not depend on the gradient terms:

$$-\frac{\partial^2 E_y}{\partial z^2} - \frac{\varepsilon(z)\omega^2}{c^2}E_y = -k^2 E_y \quad (2)$$

However, as demonstrated in [3], surface wave-like solutions of the latter equation may also exist for some realistic near-surface $\varepsilon(z)$ distributions at the water-air interface

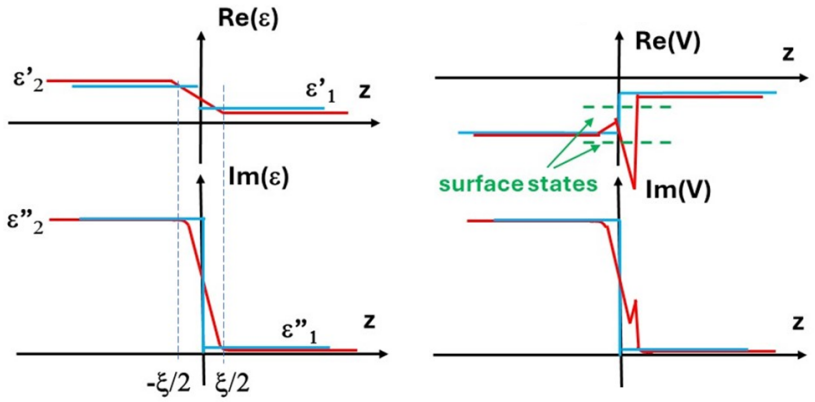

FIGURE 1. Schematic diagram of real and imaginary parts of the effective potential $V(z)$ resulting from a linear transition region (see Eq. (4)) between a highly lossy medium and a good dielectric. The red line plots correspond to the linear transition case, while the blue line plots correspond to a sharp step-like transition.

If the gradient terms in Eq. (1) are disregarded, and the interface between two media having dielectric permittivity ε_1 and ε_2 is assumed to be infinitely sharp, the SEW wavevector for the TM-polarized wave equals [2]:

$$k_{SW} = \frac{\omega}{c}\left(\frac{\varepsilon_1\varepsilon_2}{\varepsilon_1+\varepsilon_2}\right)^{1/2} \tag{3}$$

In the case of a highly lossy conductive medium having large imaginary ε_2 (such as water or biological tissues in the radio frequency (RF) range) bounding a low loss dielectric having real positive ε_1, the wavevector given by Eq. (3) is almost real. This well-known SEW solution is called Zenneck wave [5]. However, since k_{SW} given by Eq. (3) is smaller than the wavevector of free photons k_{ph} in the dielectric medium ε_1, Zenneck wave existence has been questioned [6].

Let us demonstrate that the influence of dielectric gradient terms in Eq. (1) makes Zenneck waves a "conventional" surface wave solution having $k_{SW} > k_{ph} = \varepsilon_1^{1/2}\omega/c$. Let us consider the simplest possible case of a "linear" transition region between the two media (the applicability of this approximation is justified by simulations in [3]):

$$\varepsilon(z) = \frac{\varepsilon_1+\varepsilon_2}{2} + \frac{\varepsilon_1-\varepsilon_2}{\xi}z, \tag{4}$$

where ξ is the width of the transition region. Based on Eq. (1), the corresponding $V(z)$ equals

$$V(z) = -\left(\frac{\varepsilon_1+\varepsilon_2}{2}+\frac{\varepsilon_1-\varepsilon_2}{\xi}z\right)\frac{\omega^2}{c^2} + \frac{3\left(\varepsilon_1-\varepsilon_2\right)^2}{4\xi^2\left(\frac{\varepsilon_1+\varepsilon_2}{2}+\frac{\varepsilon_1-\varepsilon_2}{\xi}z\right)^2} \tag{5}$$

A schematic diagram of the resulting potential is presented in Fig. 1 assuming

$$\varepsilon"_2 >> \varepsilon'_2 >> \varepsilon'_1 >> \varepsilon"_1 \tag{6}$$

It is easy to observe that near $z = \xi/2$ the effective potential equals

$$V(z) \approx -\varepsilon_1\frac{\omega^2}{c^2} + \frac{3\left(\varepsilon_1-\varepsilon_2\right)^2}{4\xi^2\varepsilon_1^2} \approx -\frac{3\varepsilon"_2^2}{4\xi^2\varepsilon'^2_1} + \frac{3\varepsilon"_2 3\varepsilon'_2}{2\xi^2\varepsilon'^2_1}i, \tag{7}$$

resulting in a deep near-surface potential well, which pushes the Zenneck state down into the $k_{\rm SW} > k_{\rm ph}$ range, and potentially leading to the appearance of additional GSEW modes [4], as illustrated by the dashed green lines in Fig. 1. Indeed, in the shallow well approximation the GSEW state may be found as

$$-k^2 \approx -\frac{1}{2}\left(\int_{-\infty}^{\infty} dz V(z)\right)^2 \approx -\frac{9}{512}\frac{\varepsilon"_2^4}{\xi^2\varepsilon'^4_1} \tag{8}$$

Depending on the detailed profile of the transition $\varepsilon(z)$ region between the two media, the GSEW state may be located either below the light line $\varepsilon_2^{1/2}\omega/c$ in the lossy medium ε_2 (as indicated by the top green line in Fig. 1) or above the light line (see the bottom green line). Regardless of the exact position, the Zenneck-like SEW states will look very similar to surface plasmons [2], whose fields decay exponentially away from the interface in both bounding media. Since surface plasmons are known for greatly increased surface sensitivity and promising bioimaging applications (due to their deep subwavelength characteristics in the visible range), a similar performance advantage may be expected from GSEWs.

The goal of the experiments described in the next sections of this paper is to initiate the practical exploration of biosensing and bioimaging applications of these newly discovered GSEWs in the RF range. Due to momentum conservation parallel to the interface, the GSEW states cannot be efficiently excited from free space using conventional far-field sources, such as conventional antennas of various kinds. In Sections 3 and 4, we study GSEW excitation and propagation by novel means, such as RF plasmonic antennas [7], which break momentum conservation parallel to the interface, and horn antennas used in the Otto geometry [8], which is well known in visible range plasmonics.

3. EXCITATION AND PROPAGATION OF GSEW LAUNCHED BY PLASMONIC ANTENNAS

The excitation of GSEWs on metal surfaces using SEW (plasmonic) antennas has been described in detail in [7]. As men-

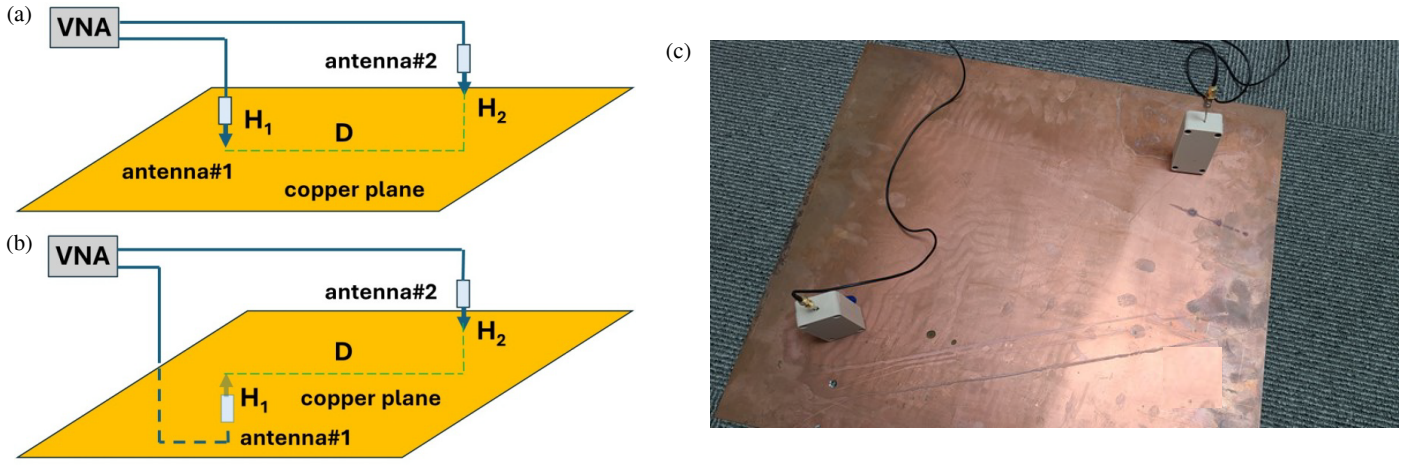

FIGURE 2. (a), (b) Experimental configurations used to study GSEW excitation and propagation on such conductive surfaces as various metals, water and human skin. A photo of plasmonic antennas positioned near a copper plane is shown in (c). The copper plate dimensions are 60 cm × 60 cm.

tioned above, the purpose of plasmonic antenna is to break the conservation of the momentum component parallel to the interface, thus making GSEW excitation possible. In this work, we extend this study to explore excitation and propagation of GSEWs on such diverse conductive surfaces such as metals, water, and human skin. The geometries of these experiments are depicted in Fig. 2. Plasmonic antennas operating in the Wi-Fi 2.45 GHz band [7] were positioned at different heights H and distances D from each other either on the same side of a conductive surface (Fig. 2(a)) or on the opposite sides of a conductive plane (Fig. 2(b)). An example of such an experimental arrangement is presented in the photo in Fig. 2(c). Plasmonic antennas were connected to the S_{11} and S_{21} ports of a portable vector network analyzer (VNA) VNA6000 introduced by NanoRFE. The measured performance of plasmonic antennas was compared to the performance of conventional dipole antennas in the same experimental configurations.

An example of such experimental data measured in the case of a pair of plasmonic antennas located near a copper plane (at $H = 0$) is presented in Figs. 3(a) and (b). A sharp GSEW excitation peak is observed in the S_{11} channel in the Wi-Fi band. This GSEW signal is clearly observed in the S_{21} channel received by the second plasmonic antenna. The deep anti-resonance features, which appear in the S_{21} channel above and below the GSEW resonance should also be noted. It will become apparent from the discussion in Section 5 that such anti-resonant features show considerable promise in sensing applications of gradient surface electromagnetic waves.

When the second plasmonic antenna was replaced by a conventional dipole antenna located at $H = 5$ cm above the copper plane, the measured S_{21} signal exhibited a very strong polarization dependence — see Fig. 3(c). This strong polarization dependence is consistent with the expected TM characteristics of the emitted GSEW. In the case of a horizontally oriented receiving dipole antenna, the S_{21} signal was weaker by $\sim$ 15–25 dB, and it may be ascribed to random scattering.

The S_{21} dependence on the lateral distance D between the two plasmonic antennas in the case of $H = 0$ is presented in Fig. 4(a) using the log-log scale. As illustrated by the 2D (red) and 3D (green) linear fits, the measured S_{21} (D) dependence may be reasonably approximated by a 2D propagation model $S_{21} \sim 1/D$, as opposed to the 3D case in which $S_{21} \sim 1/D^2$ would be expected. The GSEW communication mechanism between plasmonic antennas was also confirmed by measuring the vertical distance dependence $S_{21}(H)$ at a fixed lateral antenna distance D, as illustrated in Fig. 4(b). The measured exponential attenuation of the $S_{21}(H)$ signal is also consistent with GSEW emission.

Since GSEW signals may propagate around a conductive plane (due to considerable coupling of surface modes which exist on the opposite sides of the plane [9]), plasmonic antennas may accomplish a seemingly "impossible" task of communicating and sensing through conductive surfaces. This was confirmed by experiments conducted in the geometry depicted in Fig. 2(b). As illustrated in Fig. 5 for the cases of 1 mm thick copper plate and 25 mm thick layer of tap water, plasmonic antennas consistently outperform conventional dipole antennas in this configuration by at least 20–25 dB margin (note that the S_{11} curves measured near copper and near water surfaces exhibit considerable shift in plasmonic resonance frequencies — comparing Figs. 5(a) and 5(c)). In addition to better coupling of plasmonic antennas located on the opposite sides of a conductive plane, another important contributing factor in these experiments is the greatly reduced efficiency of conventional dipole antennas if they are placed near a conductive surface.

The ability to excite GSEWs on the surface of water has important implications for biosensing and bioimaging. Indeed, since the human body is mostly made of water, the observation of surface wave excitation and propagation on the water surface (demonstrated in Figs. 5(c) and (d)) implies that plasmonic antennas may be used to excite and propagate GSEW signals on various human body parts. Such an experiment is depicted in Fig. 6 where GSEW signals were propagated along the length of a human arm. The S_{11} and S_{21} plots in Fig. 6 appear rather similar to plasmonic resonances and anti-resonances observed on other conductive surfaces (see Figs. 3 and 5). Moreover,

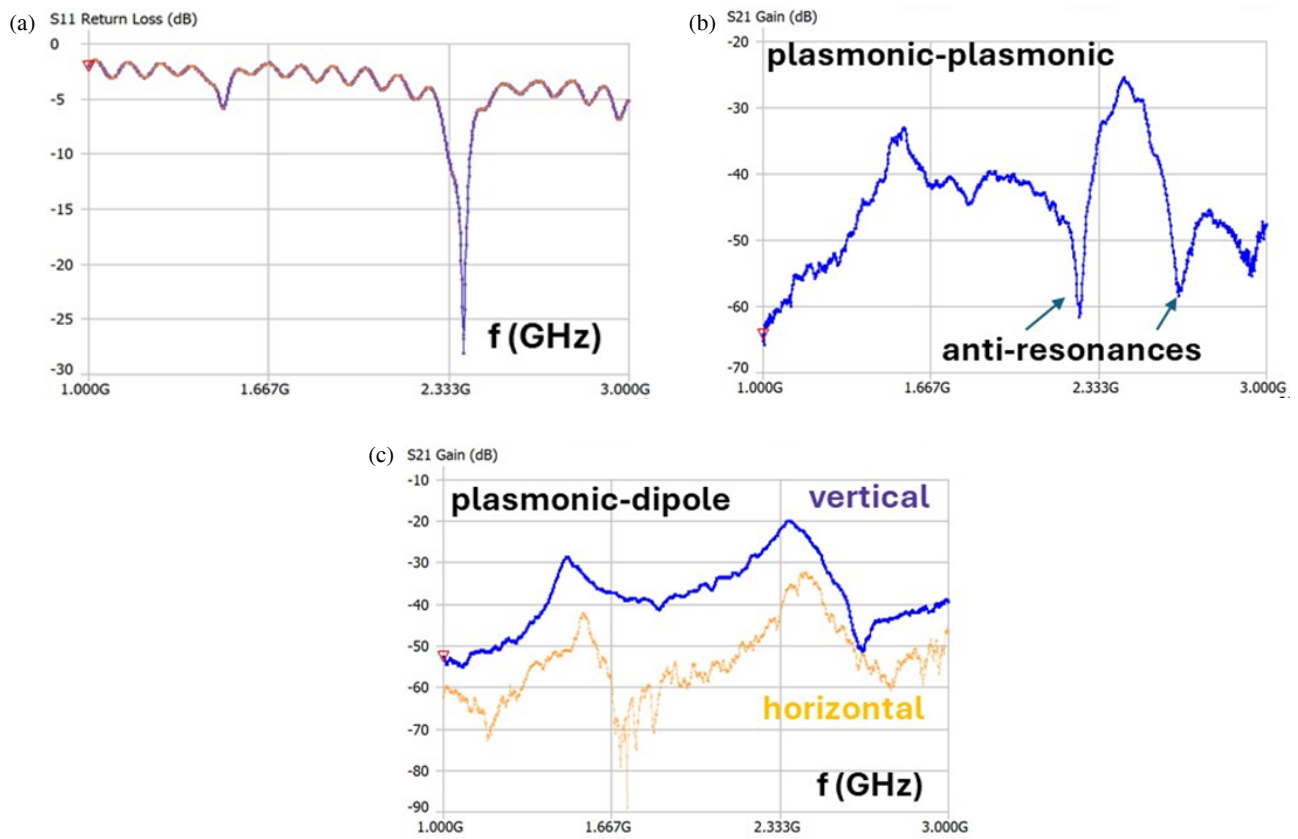

FIGURE 3. An example of S_{11} (a) and S_{21} signals measured for (b) a pair of plasmonic antennas located near a copper plane (at $H = 0$, $D = 10$ cm), and for a plasmonic-dipole antenna combination (c). A sharp GSEW excitation peak is observed in the S_{11} channel in the WI-FI band. In the case of a plasmonic antenna pair (b), sharp anti-resonances are observed in the S_{21} channel above and below the resonant frequency. In the case of a conventional dipole antenna located at $D = 5$ cm at $H = 5$ cm above the copper plane (c) the S_{21} signal exhibits strong polarization dependence consistent with the surface wave character of plasmonic antenna emission.

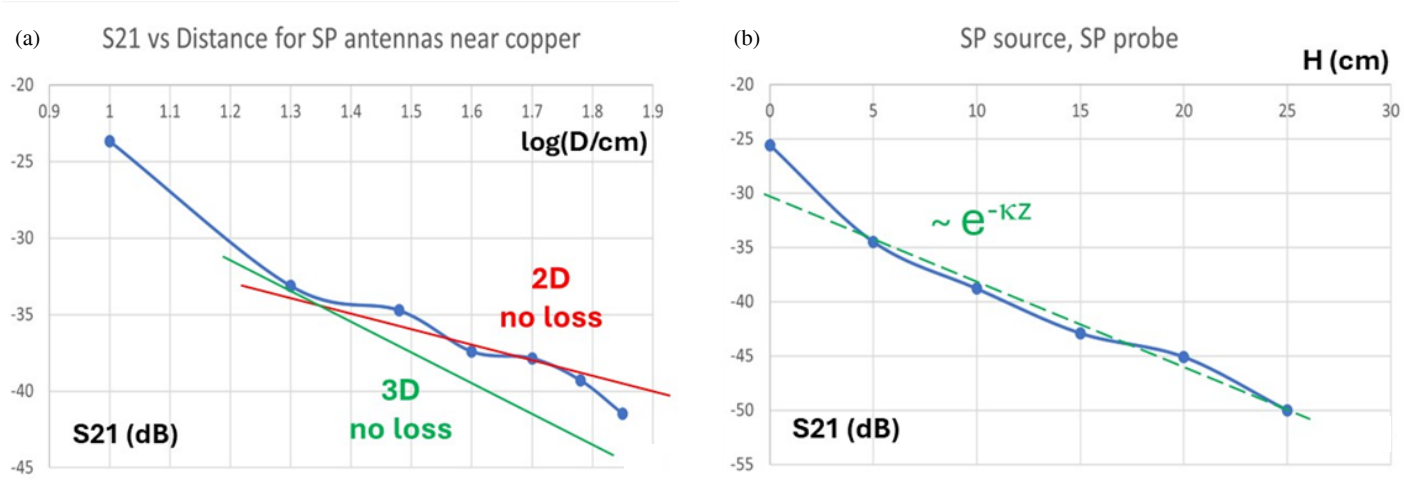

FIGURE 4. (a) Attenuation of S_{21} signal as a function of D measured in the WI-FI band for two plasmonic antennas located at $H = 0$. The measured S_{21} (D) dependence may be approximated by a 2D propagation model. (b) The S_{21} dependence on vertical distance H measured at fixed lateral distance $D = 10$ cm between two plasmonic antennas exhibits a clear exponential behavior consistent with GSEW emission.

the $S_{21}(H)$ and $S_{21}(D)$ curves measured near a human hand also appear quite similar, which strongly indicates the surface wave origins of the observed signals. In particular, similar to results obtained on a copper plane, the measured $S_{21}(D)$ dependence may be approximated by a 2D propagation model (compare Fig. 4(a) and Fig. 6(d)). GSEW sensing experiments conducted using the described approach in various bio-inspired configurations will be described in detail later in Section 5.

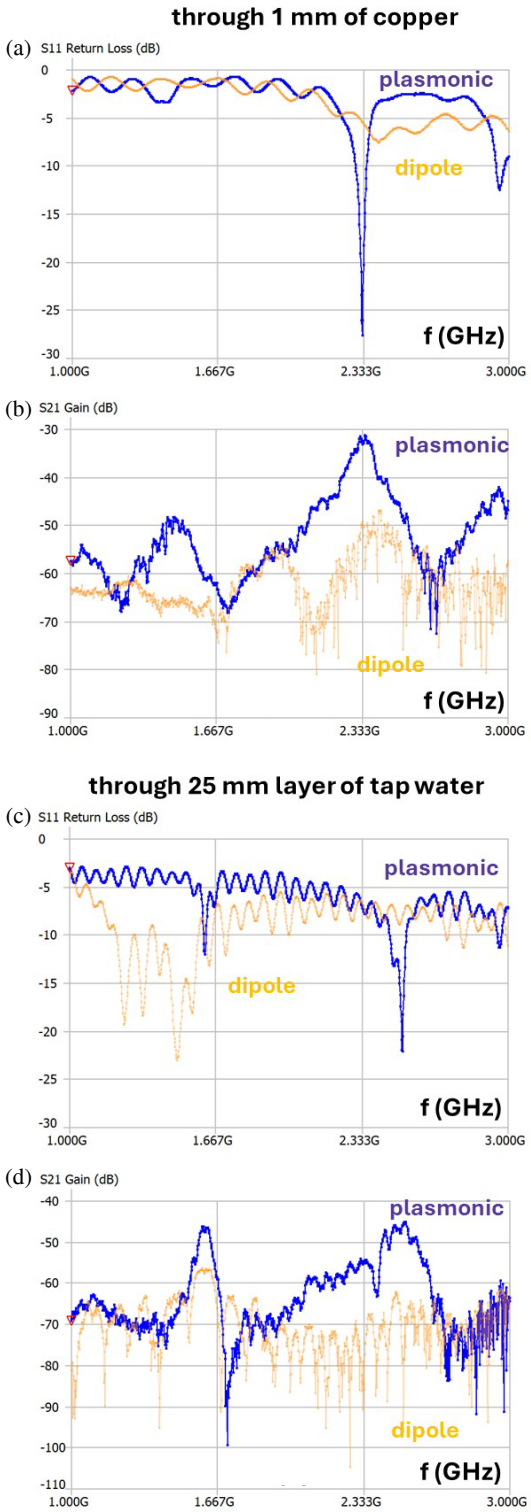

FIGURE 5. Examples of S_{11} and S_{21} signals measured in the geometry depicted in Fig. 2(b) for a pair of identical antennas separated by a 1 mm thick copper plate (a), (b), and 25 mm thick layer of tap water (c), (d). The blue curves correspond to plasmonic WI-FI antennas, while yellow curves correspond to conventional dipole WI-FI antennas. The plasmonic antennas outperform the conventional ones by 20–25 dB margin.

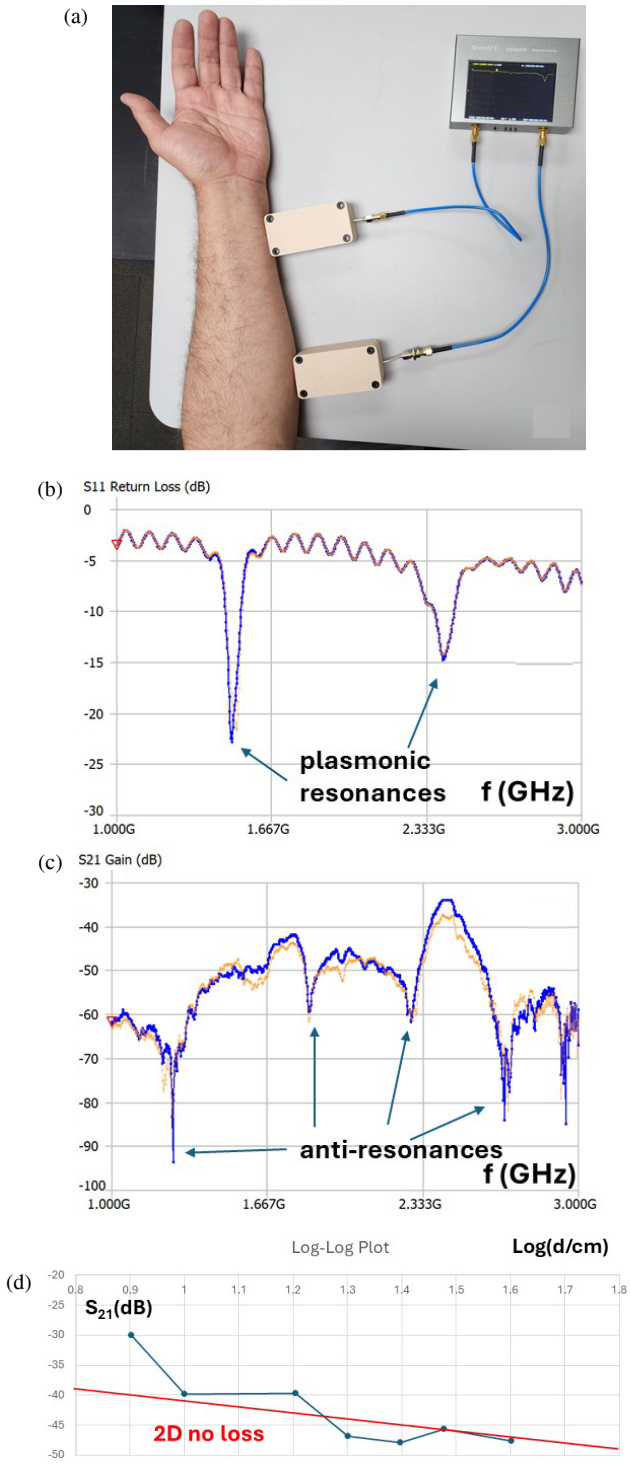

FIGURE 6. (a) Photo of surface wave excitation and propagation experiment using plasmonic WI-FI antennas positioned near a human hand. The S_{11} (b) and S_{21} (c) curves measured by a VNA (which are averaged over 10 successive measurement runs) exhibit plasmonic resonances and anti-resonances which look similar to the data obtained on other conductive surfaces such as tap water. (d) Attenuation of S_{21} signal as a function of D measured in the WI-FI band for two plasmonic antennas located near the hand. The measured S_{21} (D) dependence may be approximated by a 2D propagation model.

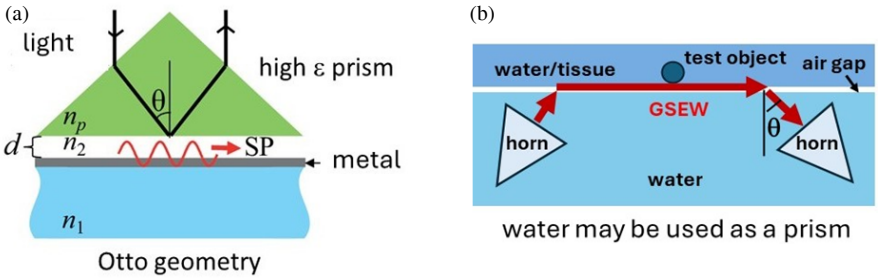

FIGURE 7. (a) The Otto configuration [8] enables excitation of surface plasmons (SP) on a metal surface across an air gap The phase matching angle θ is established between the incident photons and the surface plasmons propagating along the metal-air interface. (b) The modified Otto geometry enables GSEW excitation on a water or biological tissue surface across a dielectric (air) gap. A pair of horn antennas filled with water and operated underwater at a phase matching angle θ is used as an excitation source and a detector of GSEWs.

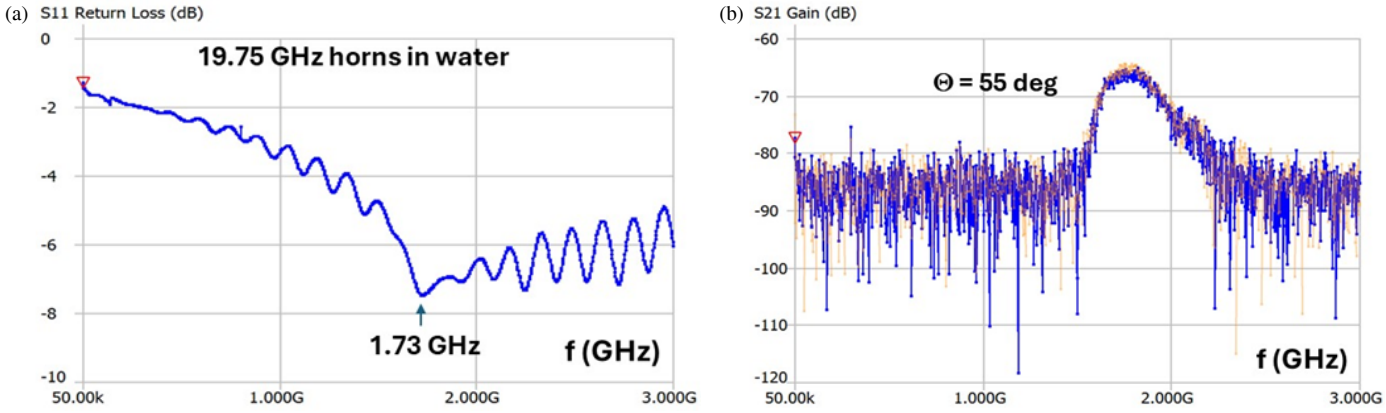

FIGURE 8. Measured S_{11} and S_{21} signals for a pair of horn antennas placed underwater in the Otto configuration. The S_{21} signal is measured at $\Theta = 55$ deg with respect to the water surface (see Fig. 7(b)). Two measurement runs are shown by blue and yellow to illustrate reproducibility.

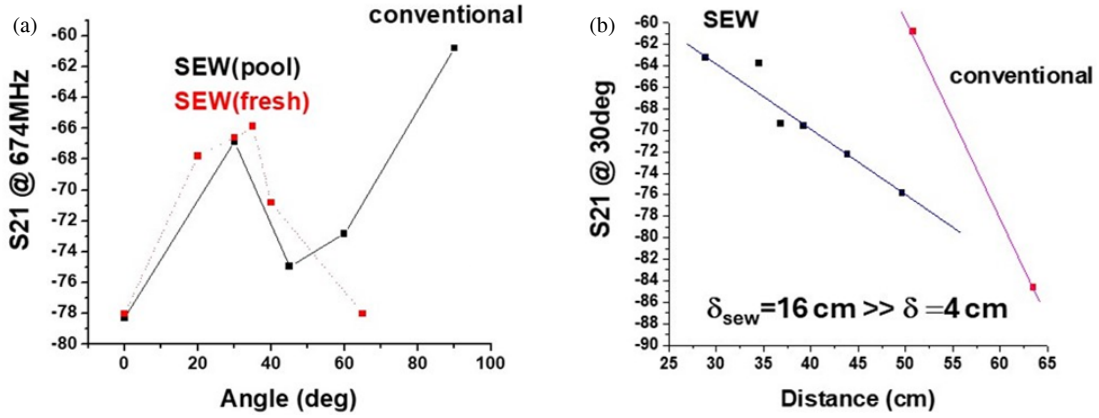

FIGURE 9. (a) S_{21} (θ) dependencies measured at 674 MHz in the Otto configuration in the fresh (red) and pool (black) water environments. In both cases the S_{21} (θ) dependencies show local maxima around $\theta = 35$ deg, which may be explained by phase-matching conditions between GSEW and the directional emission from the horns. (b) Attenuation of the GSEW signal measured at $\theta = 30$ deg as a function of distance between the horns underwater (black) is compared to the attenuation of the conventionally propagated signal (red) measured between the horns pointed directly at each other at $\theta = 90$ deg. The measured attenuation constant $\delta = 4$ cm of the conventional signal equals the skin depth in water at 674 MHz, while the attenuation constant of the GSEW signal $\delta_{\mathbf{SEW}} = 16$ cm appears to be considerably larger.

4. EXCITATION AND PROPAGATION OF GSEW LAUNCHED BY HORN ANTENNAS

Unlike plasmonic antennas, which break momentum conservation parallel to the interface, the use of Otto geometry depicted in Fig. 7(a) (see for example Ref. [8]) enables direct phase matching between a far-field plane wave source and a surface electromagnetic wave. In the classical Otto geometry, the use of high refractive index prism enables the phase matching between the large-momentum photons in the prism and surface plasmons propagating over the metal-air interface (recall

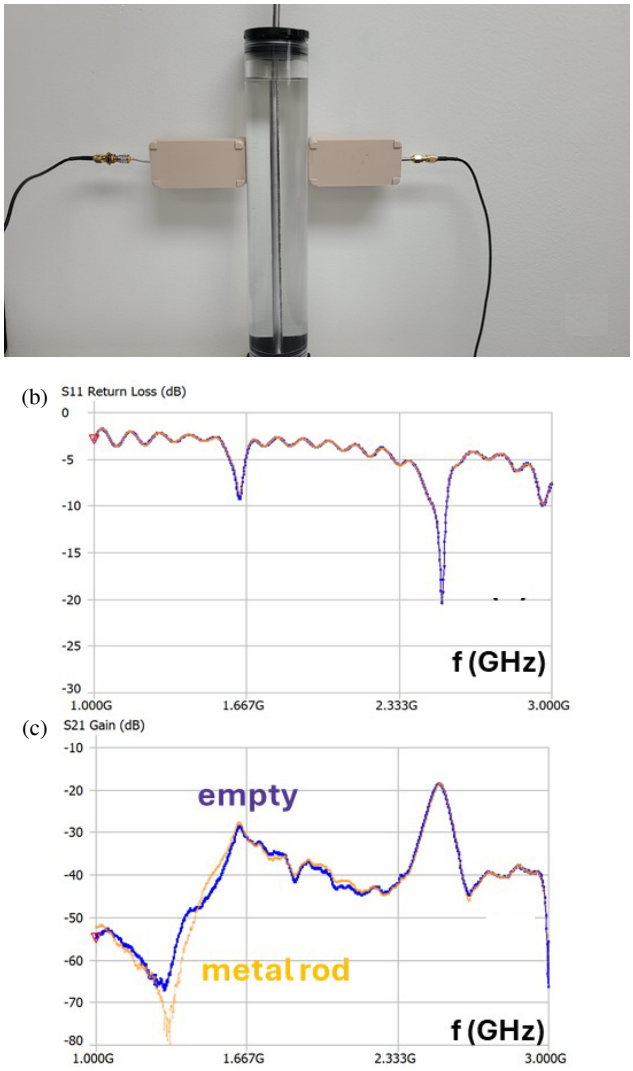

FIGURE 10. (a) Photo of a surface wave excitation experiment using plasmonic antennas positioned near a water-filled plastic cylinder. The measured S_{11} (b) and S_{21} (c) curves exhibit plasmonic resonances and anti-resonances which look similar to the data obtained on a human hand — see Fig. 6. The data shown in (c) compare measured S_{21} before and after insertion of a metal rod in the middle of the cylinder. The S_{21} signal changes considerably near the plasmonic anti-resonance observed around 1.3 GHz.

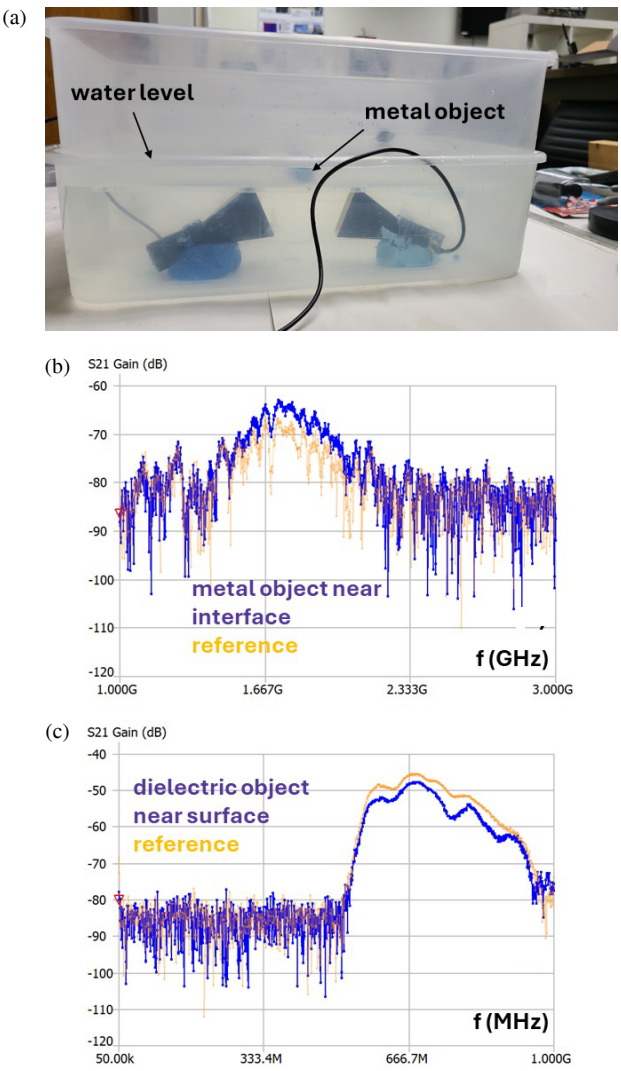

FIGURE 11. (a) Photo of a surface wave excitation experiment conducted in the Otto geometry (see Fig. 7(b)) using the 1.7 GHz underwater horn antennas. The two plastic containers seen in the photo were filled with tap water. The bottom of the upper container played the role of a dielectric gap. (b) Comparison of the S_{21} signal measured in this experimental configuration with (blue) and without (yellow) a metal object inside the water layer. (c) A similar experiment performed using the 670 MHz horns with a dielectric object near water surface.

that plasmon momentum is larger than the photon momentum in the air, so that direct excitation of plasmons from free space is impossible [2]). In the modified Otto geometry depicted in Fig. 7(b), the same goal is accomplished by placing the directional RF horn antennas underwater. By varying the angular orientation of the horns, the phase matching conditions may be achieved between the directional radio waves emitted by the horn and the GSEW propagating over the water-air (or tissue-air) interface. Note that the air gap geometry shown in both interfaces of Figs. 7(a) and (b) may support GSEW propagation.

Our experiments with underwater horn antennas were conducted using two sets of commercial of-the-shelf horns which were originally designed for free space operation and filled with water. The first set was designed for free space operation in the 5150–6400 MHz frequency band (RF Elements, model number STH-A45-USMA). When being filled with water and operated in tap water and pool water environments, the operating band of these horns shifted down to 650–820 MHz. The second set (Chengdu Xixia Technology Development Co, model number XEXA076) was designed for free space operation in the 19.8–23.1 GHz band. When being used underwater, its operating frequency shifted down to 1.7–2.3 GHz band. An example of a horn pair characterization underwater performed in the Otto configuration is shown in Fig. 8.

The measured angular S_{21} (θ) dependences obtained in the fresh and pool water environments were similar to each other, as indicated in Fig. 9(a). They showed considerable coupling

improvement under the phase matching conditions between the directional emission from the horns and GSEWs propagating over the water-air interface. The GSEW peak was observed in the $\theta = 30$–40 degrees range. The amplitude of this peak was measured as a function of distance between the horns underwater, as shown in Fig. 9(b). It was compared to the conventionally propagated signal which was measured underwater between the horns pointed directly at each other (at $\theta = 90$ degrees). The attenuation constant $\delta = 4$ cm of the conventional signal coincided with the skin depth in water at 674 MHz. On the other hand, similar to our previous results obtained at 30 MHz [10], the measured attenuation constant of the GSEW signal was considerably larger ($\delta_{SEW} = 16$ cm). We should also mention that surface electromagnetic waves may also be potentially excited by other means, as for example described in [11].

5. EXPERIMENTS PERFORMED IN EMULATED BIOSENSING GEOMETRIES

In the experiments described in Sections 3 and 4, we demonstrated our ability to excite and propagate GSEW on various water-air and tissue-air interfaces. Let us now demonstrate the capability of GSEW-based techniques to detect the presence of metallic and dielectric objects underwater in close proximity to the water surface. Since biological tissues are mostly made of water, the configuration of our experiments closely emulates various potential biosensing and bioimaging applications of GSEW.

A surface wave excitation experiment performed using plasmonic antennas positioned near a water-filled plastic cylinder is depicted in Fig. 10. As illustrated by the measured S_{11} (see Fig. 10(b)) and S_{21} (see Fig. 10(c)) signals, a water-filled plastic cylinder exhibits a set of plasmonic resonances and anti-resonances which look quite similar to the data obtained on a human arm (compare Fig. 10 with Fig. 6). Moreover, as illustrated in Fig. 10(c) the measured S_{21} signal may be used to detect the insertion of a metal rod in the middle of the water-filled cylinder. The S_{21} signal changes considerably near the plasmonic anti-resonance observed around 1.3 GHz. The observed 15 dB change corresponds to about a factor of 3, which is quite adequate for medical imaging purposes. These experiments indicate the potential ability of GSEW-based techniques to detect a foreign object or unwanted lump inside a biological tissue.

We also conducted similar underwater object detection experiments in the Otto geometry depicted in Fig. 7(b). A photo of such an experimental arrangement can be seen in Fig. 11(a) in which the 1.7 GHz underwater horns were used. The two plastic containers seen in the photo were filled with tap water. The bottom of the upper container played the role of a dielectric gap. As illustrated in Fig. 11(b), a metal object (4.5 cm long, 1 cm diameter) placed inside the upper water layer is easily detectable in the Otto configuration. Similar experiments conducted with 670 MHz underwater horns were equally successful. Results of such an experiment performed using a dielectric object located near water surface are shown in Fig. 11(c). In both cases shown in Figs. 11(b) and (c), the S_{21} signal is changed by 5–10 dB in the operational band of the respective horn antennas.

6. CONCLUSIONS

In summary, in this paper we present theoretical and experimental studies of gradient surface electromagnetic wave excitation and propagation on such conductive surfaces as various metals, water, and human organs. The geometry of our experiments was motivated by various biosensing applications of surface electromagnetic waves in the visible range [12, 13], and it was designed to emulate various potential biosensing and bioimaging applications of GSEW. We demonstrate the capability of GSEW-based techniques to communicate and sense through conductive surfaces, and to detect the presence of metallic and dielectric objects underwater in close proximity to the water surface. Since the dielectric properties of human tissue are similar to those of water, we anticipate that the developed GSEW technique may supplement X-ray and ultrasound-based biosensing and bioimaging.

REFERENCES

[1] Smolyaninov, I. I., "Surface electromagnetic waves at gradual interfaces between lossy media," *Progress In Electromagnetics Research*, Vol. 170, 177–186, 2021.

[2] Zayats, A. V., I. I. Smolyaninov, and A. A. Maradudin, "Nano-optics of surface plasmon polaritons," *Physics Reports*, Vol. 408, No. 3-4, 131–314, 2005.

[3] Smolyaninov, I. I., Q. Balzano, and A. B. Kozyrev, "Surface electromagnetic waves at seawater-air and seawater-seafloor interfaces," *IEEE Open Journal of Antennas and Propagation*, Vol. 4, 51–59, 2022.

[4] Smolyaninov, I. I., "Surface electromagnetic waves in lossy conductive media: Tutorial," *Journal of the Optical Society of America B*, Vol. 39, No. 7, 1894–1901, 2022.

[5] Michalski, K. A. and J. R. Mosig, "The Sommerfeld half-space problem revisited: From radio frequencies and Zenneck waves to visible light and Fano modes," *Journal of Electromagnetic Waves and Applications*, Vol. 30, No. 1, 1–42, 2016.

[6] Kukushkin, A. V., "On the existence and physical meaning of the Zenneck wave," *Physics-Uspekhi*, Vol. 52, No. 7, 755, 2009.

[7] Smolyaninov, I. I., Q. Balzano, and D. Young, "Surface wave-based radio communication through conductive enclosures," *Progress In Electromagnetics Research M*, Vol. 85, 21–28, 2019.

[8] Akowuah, E. K., T. Gorman, and S. Haxha, "Design and optimization of a novel surface plasmon resonance biosensor based on otto configuration," *Optics Express*, Vol. 17, No. 26, 23 511–23 521, 2009.

[9] Ebbesen, T. W., H. J. Lezec, H. F. Ghaemi, T. Thio, and P. A. Wolff, "Extraordinary optical transmission through sub-wavelength hole arrays," *Nature*, Vol. 391, No. 6668, 667–669, 1998.

[10] Smolyaninov, I. I., Q. Balzano, M. Barry, and D. Young, "Superlensing enables radio communication and imaging underwater," *Scientific Reports*, Vol. 13, No. 1, 18333, 2023.

[11] Zou, D., C. Tu, and C. Cui, "Helical streamers guided by surface electromagnetic standing waves," *Plasma Science and Technology*, Vol. 25, No. 7, 072001, 2023.

[12] Mejía-Salazar, J. R. and O. N. Oliveira Jr., "Plasmonic biosensing," *Chemical Reviews*, Vol. 118, No. 20, 10 617–10 625, 2018.

[13] Li, M., S. K. Cushing, and N. Wu, "Plasmon-enhanced optical sensors: A review," *Analyst*, Vol. 140, No. 2, 386–406, 2015.